THE JOURNAL OF BIOLOGICAL CHEMISTRY
Vol. 279, No. 22, Issue of May 28, pp. 23431–23437, 2004
Printed in U.S.A.

Molecular Structure of Human Galactose Mutarotase*

Received for publication, March 2, 2004, and in revised form, March 12, 2004
Published, JBC Papers in Press, March 16, 2004, DOI 10.1074/jbc.M402347200

James B. Thoden‡, David J. Timson§, Richard J. Reece¶, and Hazel M. Holden‡‖

From the ‡Department of Biochemistry, University of Wisconsin, Madison, Wisconsin 53706, §School of Biology and Biochemistry, Medical Biology Centre, Queen's University Belfast, 97 Lisburn Road, Belfast BT9 7BL, United Kingdom, and ¶School of Biological Sciences, The Michael Smith Building, The University of Manchester, Oxford Road, Manchester M13 9PT, United Kingdom

Galactose mutarotase catalyzes the conversion of β-D-galactose to α-D-galactose during normal galactose metabolism. The enzyme has been isolated from bacteria, plants, and animals and is present in the cytoplasm of most cells. Here we report the x-ray crystallographic analysis of human galactose mutarotase both in the apoform and complexed with its substrate, β-D-galactose. The polypeptide chain folds into an intricate array of 29 β-strands, 25 classical reverse turns, and 2 small α-helices. There are two *cis*-peptide bonds at Arg-78 and Pro-103. The sugar ligand sits in a shallow cleft and is surrounded by Asn-81, Arg-82, His-107, His-176, Asp-243, Gln-279, and Glu-307. Both the side chains of Glu-307 and His-176 are in the proper location to act as a catalytic base and a catalytic acid, respectively. These residues are absolutely conserved among galactose mutarotases. To date, x-ray models for three mutarotases have now been reported, namely that described here and those from *Lactococcus lactis* and *Caenorhabditis elegans*. The molecular architectures of these enzymes differ primarily in the loop regions connecting the first two β-strands. In the human protein, there are six extra residues in the loop compared with the bacterial protein for an approximate longer length of 9 Å. In the *C. elegans* protein, the first 17 residues are missing, thereby reducing the total number of β-strands by one.

During normal galactose metabolism, β-D-galactose is converted to glucose 1-phosphate via the action of four enzymes that constitute the Leloir pathway as shown in Scheme 1 (1). In the first step of this pathway, β-D-galactose is epimerized to α-D-galactose through the action of galactose mutarotase. The second step involves the phosphorylation of α-D-galactose to galactose 1-phosphate by galactokinase. As indicated in Scheme 1, galactose 1-phosphate uridylyltransferase catalyzes the third step by transferring a UMP group from UDP-glucose to galactose 1-phosphate, thereby generating glucose 1-phosphate and UDP-galactose. To complete the pathway, UDP-galactose is converted to UDP-glucose by UDP-galactose 4-epimerase.

Mutations in three of the enzymes of the Leloir pathway, namely galactokinase, galactose 1-phosphate uridylyltransferase, or UDP-galactose 4-epimerase, have been demonstrated to result in the diseased state known as galactosemia (2, 3). The symptoms of this genetic disease include early onset cataracts (typically within the first two years of life) and, in more severe cases, liver, kidney, and brain damage. Cataract formation is believed to be caused by the buildup of unmetabolized galactose in the lens of the eye. Aldose reductase catalyzes the reduction of the sugar to galactitol (dulcitol), which is not, in contrast to galactose, readily transported across the plasma membrane (4–6). As such, the accumulation of this highly osmotically active compound draws excess water into the lens resulting in cataracts by a mechanism that is not fully understood. The more severe symptoms of galactosemia are most likely caused by a combination of these osmotic effects and the accumulation of the intermediate α-D-galactose-1-phosphate (7), although the precise mechanism of toxicity is not understood. No known disease-causing mutations in human galactose mutarotase have been identified thus far. However, galactitol is reported to be an inhibitor of mammalian mutarotase (8), raising the possibility that its accumulation would partly block the action of mutarotase, resulting in a further buildup of unmetabolized galactose.

Galactose mutarotase activity was first reported in *Escherichia coli* in 1965 (9) and has since been observed in a wide range of organisms, including bacteria (9–16), plants (17, 18), fungi (19), and mammals (20–23). It is present in the cytoplasm of most cells, suggesting that the *in vivo* rate of uncatalyzed mutarotation is insufficient for the metabolic needs of the organism. Indeed, deletion of the mutarotase gene from *E. coli* results in slow growth on minimal medium containing phenyl-β-D-galactopyranose as the sole carbon source (11).

The first three-dimensional structure of a dimeric mutarotase, namely that from *Lactococcus lactis*, was reported in 2002 (24). The enzyme was shown to adopt a β-sandwich motif, similar to that seen in domain 5 of β-galactosidase (25) with the sugar binding site located in a wide, shallow cleft. Five highly conserved residues (Arg-71, His-96, His-170, Asp-243, and Glu-304) were within hydrogen-bonding distance to the hydroxyl groups of the bound galactose ligand. Previous kinetic studies suggested that the reaction mechanism for the enzyme proceeds via an acid/base mechanism with a transient ring opening (26, 27), and the model of the mutarotase from *L. lactis* implicated Glu-304 as the likely catalytic base and either His-96 or His-170 as the catalytic acid (24). Accordingly, the reaction mechanism of galactose mutarotase is thought to occur via abstraction of the proton from the C-1 hydroxyl group by Glu-304 in the *L. lactis* enzyme and protonation of the ring oxygen of the sugar by His-170, which results in ring opening. Subsequent rotation about the C-1–C-2 bond followed by a

* This research was supported in part by National Institutes of Health Grant DK47814 (to H. M. H.) and a grant from The Wellcome Trust (to R. J. R.). The costs of publication of this article were defrayed in part by the payment of page charges. This article must therefore be hereby marked "*advertisement*" in accordance with 18 U.S.C. Section 1734 solely to indicate this fact.

The atomic coordinates and structure factors (codes 1SNZ and 1SO0) have been deposited in the Protein Data Bank, Research Collaboratory for Structural Bioinformatics, Rutgers University, New Brunswick, NJ (http://www.rcsb.org/).

‖ To whom correspondence should be addressed. Tel.: 608-262-4988; Fax: 608-262-1319; E-mail: Hazel_Holden@biochem.wisc.edu.

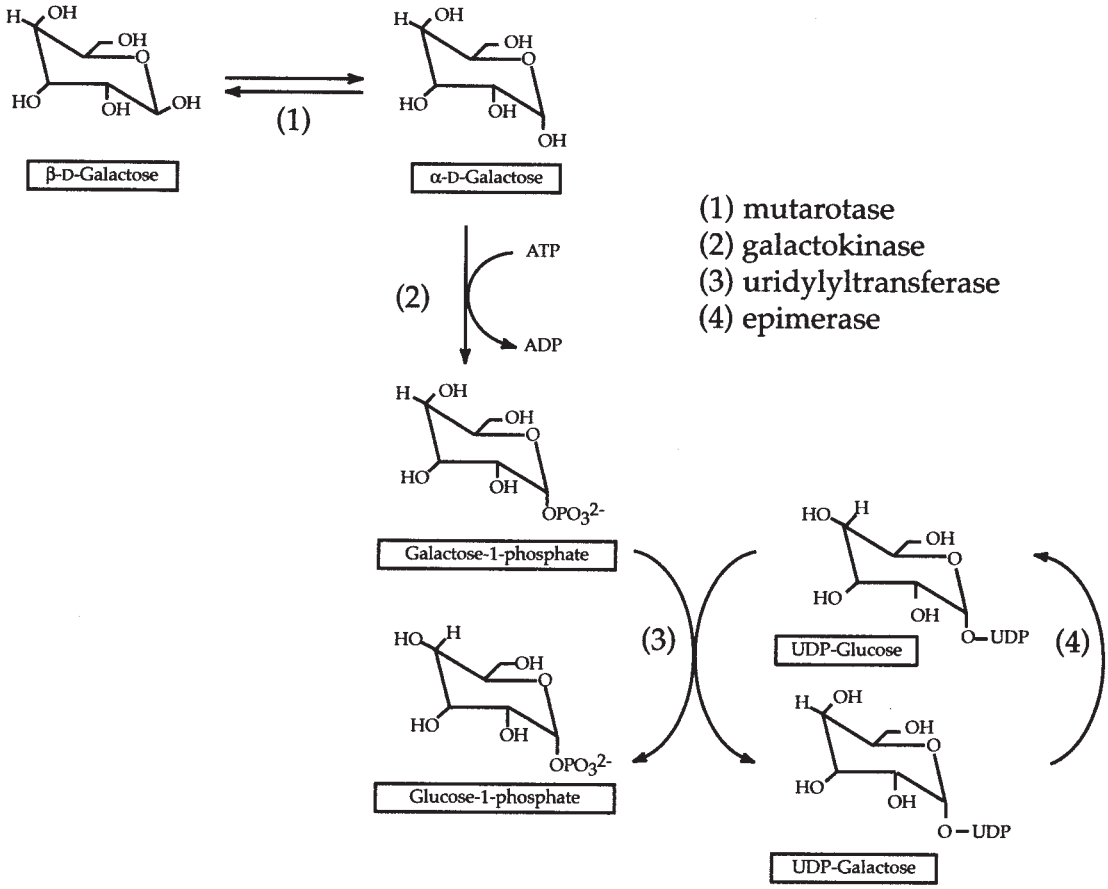

SCHEME 1

reversal of the ring opening events ultimately yields a product with an altered configuration at C-1 (28). Site-directed mutagenesis of these residues (or their equivalents in the *E. coli* enzyme) have confirmed the role of Glu-304 as the catalytic base and established His-170 as the catalytic acid (28, 29).

The gene encoding the human enzyme was identified in 2003, and the protein product was characterized (30). From these investigations, it was suggested that Glu-307 and His-176 fulfill the roles in acid/base catalysis in the human mutarotase (30). Interestingly, regardless of the source, mutarotases tend to show a preference for galactose over glucose and have high k_{cat} and K_m values with this sugar (typically $10^4 - 10^5$ s^{-1} and 10 − 100 mM, respectively) (23, 30–33). The preference of these enzymes for galactose over glucose was addressed structurally with the *L. lactis* mutarotase and, at least in the case of this bacterial protein, is explained by the existence of nonproductive binding modes in the active site for glucose and its derivatives (33). With respect to quaternary structure, human mutarotase appears to be monomeric (10, 30), whereas the *L. lactis* enzyme was shown to be a dimer on the basis of ultracentrifugation experiments (24). The biochemical significance, if any, of these differences in quaternary structure is not understood at the present time.

Here we describe the three-dimensional structure of human galactose mutarotase, both in the unbound state and complexed with its substrate, β-D-galactose. This study represents the first report of a eukaryotic mutarotase with bound sugar and allows for a detailed comparison between the human and the bacterial forms of the enzyme.

EXPERIMENTAL PROCEDURES

Cloning of the Galactose Mutarotase Gene—The human galactose mutarotase gene was amplified from the originally described pET21-GALM plasmid (30) using a forward primer designed with an NdeI restriction site at the start codon and a reverse primer with a XhoI restriction site after the stop codon. This construct allowed for insertion of the PCR product into the pTYB12 expression vector, which provides an N-terminal chitin-binding domain followed by a dithiothreitol-inducible intein (New England Biolabs). The recloning was done because diffraction-quality crystals could not be obtained with protein expressed from the pET21-GALM plasmid construct, which contained a noncleavable N-terminal polyhistidine tag.

Protein Expression and Purification—For protein expression, the pTYB12-GALM plasmid was used to transform *E. coli* HMS174(DE3) cells (Novagen). A starter culture from a single colony was grown overnight at 37 °C in LB medium supplemented with ampicillin. Subsequently, 10 ml were transferred to 1000 ml of the supplemented LB medium in a 2-liter shaker flask and grown at 37 °C until an optical density of 0.8 was achieved at 600 nm. The cultures were cooled to 16 °C in an ice-water bath, and IPTG[1] was added to a final concentration of 1 mM. Cell growth was allowed to continue at 16 °C for an additional 15 h.

The cells were harvested by centrifugation at 4,000 × *g* for 15 min and frozen in liquid nitrogen. Frozen cells (50 g) were thawed in 150 ml of lysis buffer consisting of 20 mM NaH_2PO_4 and 500 mM NaCl (pH 8.0). The thawed cells were placed in an ice bath and disrupted by four rounds of sonication (1-min duration each) separated by 5 min of cooling. Cellular debris was removed by centrifugation at 20,000 × *g* for 25 min. The clarified supernatant was loaded onto a 100-ml column of chitin beads (New England Biolabs) that had been equilibrated previously with lysis buffer. The column was then washed with lysis buffer until the absorbance reading at 280 nm reached background level. The column was charged by washing with 200 ml of lysis buffer augmented with 100 mM dithiothreitol. The charged column was subsequently moved to room temperature, allowed to stand for 18 h, and then returned to 4 °C. The cleaved protein was eluted with lysis buffer. Pro-

[1] The abbreviations used are: IPTG, isopropyl-1-thio-β-D-galactopyranoside; Homopipes, homopiperazine-*N*,*N*′-bis-2-(ethanesulfonic acid); MES, 2-(*N*-morpholino)ethanesulfonic acid; r.m.s.d., root mean square deviation; PEG, polyethylene glycol.

TABLE I
X-ray data collection statistics

Data set	Resolution	Independent reflections	Completeness	Redundancy	Avg. I/Avg. $\sigma(I)$	R_{sym}[a]
	Å		%			
Apo protein	30.0−2.20	36,670	94.8	3.4	8.3	7.1
	2.30−2.20[b]	4,192	90.1	1.6	1.6	26.9
Protein-sugar complex	30.0−2.30	61,156	94.7	2.1	10.8	7.0
	2.40−2.30	5,979	77.5	1.4	2.8	26.4

[a] $R_{sym} = (\Sigma|I - \bar{I}|/\Sigma I) \times 100$.
[b] Statistics for the highest resolution bin.

TABLE II
Relevant refinement statistics

	Apoprotein	Protein-sugar complex
Resolution limits (Å)	30.0-2.20	30.0-2.30
R-factor (overall) (%)/no. reflections[a]	17.4/36,670	16.9/61,156
R-factor (working) (%)/no. reflections	17.2/33,003	16.7/55,040
R-factor (free) (%)/no. reflections	20.1/3,667	19.8/6,116
No. protein atoms	5,111[b]	10,746[c]
No. heteroatoms	258 (waters)	454[d]
Bond lengths (Å)	0.011	0.013
Bond angles (°)	2.34	2.40
Trigonal planes (Å)	0.007	0.007
General planes (Å)	0.011	0.012
Torsional angles (°)[e]	19.9	19.5

[a] R-factor = $(\Sigma|F_o - F_c|/\Sigma|F_o|) \times 100$, where F_o is the observed structure-factor amplitude and F_c is the calculated structure-factor amplitude.
[b] These include multiple conformations for Arg-30, Arg-121, and Ser-186 in monomer I and Val-75 in monomer II.
[c] These include multiple conformations for Glu-102 and Glu-229 in monomer I, Glu-229 in monomer II, and Arg-48 in monomer IV.
[d] These include four β-D-galactose moieties and 406 waters.
[e] The torsional angles were not restrained during the refinement.

tein-containing fractions were pooled based on purity, as judged by SDS-PAGE, and dialyzed against 10 mM HEPES and 200 mM NaCl (pH 7.5). The dialyzed protein was concentrated to 23.0 mg/ml based on the extinction coefficient of 0.85 $ml \cdot mg^{-1} \cdot cm^{-1}$ as calculated with the program Protean (DNASTAR, Inc., Madison, WI). A typical yield was between 80 and 100 mg of protein/50 grams of cells.

Crystallization of Apogalactose Mutarotase—A search for crystallization conditions was conducted both at room temperature and at 4 °C via the hanging drop method of vapor diffusion utilizing an in-house-designed sparse matrix screen composed of 144 conditions. The best crystals were observed growing at 4 °C from polyethylene glycol 8000 (PEG-8000) at pH 5.0. Large single crystals were subsequently obtained by seeding into batch experiments with precipitant solutions of 5–8% PEG-8000 buffered with 100 mM Homopipes (pH 5.0) and enzyme concentrations of 12 mg/ml. Diamond-shaped crystals grew to maximum dimensions of ~0.5 × 0.3 × 0.1 mm in 3–5 weeks. They belonged to the space group $P2_1$ with unit cell dimensions of a = 60.7 Å, b = 90.7 Å, c = 70.0 Å, and β = 102.5°. The asymmetric unit contained two monomers.

Structural Analysis of Apogalactose Mutarotase—An x-ray data set was collected to 2.2 Å resolution at 4 °C with a Bruker HISTAR area detector system equipped with Supper "long" mirrors. The x-ray source was CuK_α radiation from a Rigaku RU200 x-ray generator operated at 50 kV and 90 mA. The x-ray data were processed with XDS (34, 35) and internally scaled with XSCALIBRE.[2] X-ray data collection statistics are presented in Table I. The structure was solved by molecular replacement with the program AMORE (36) and using, as a search model, one subunit of the *L. lactis* enzyme (Protein Data Bank accession number 1L7J). Two peaks were readily identified in the rotation search. A subsequent translation search and rigid body refinement to 3.0 Å yielded an R-factor of 46%. To reduce model bias, the electron densities corresponding to the two monomers in the asymmetric unit were averaged with the software package AVE (37, 38). From this averaged electron density map, a model for the complete monomer was constructed and then placed back into the unit cell for subsequent least squares refinement with TNT (39). Alternate cycles of manual rebuilding and least square refinement reduced the R-factor to 17.4% for all measured x-ray data to 2.2 Å resolution. Refinement statistics are presented in Table II.

Structural Analysis of Galactose Mutarotase Complexed with β-D-Galactose—Apogalactose mutarotase crystals were harvested from batch experiments and equilibrated in a synthetic mother liquor composed of 10% PEG-8000, 200 mM NaCl, 100 mM Homopipes (pH 5.0), and 100 mM D-galactose in an attempt to soak the sugar into the crystalline lattice. This, however, led to cracking of the crystals and a marked change in lattice parameters and x-ray diffraction quality. Following these initial soaking experiments, crystals were grown by seeding into batch experiments with precipitant solutions of 5–8% PEG-8000 buffered with 100 mM MES (pH 6.0), 200 mM LiCl, and 100 mM D-galactose with enzyme concentrations of 12.0 mg/ml. The crystals of the apoenzyme were used for initial nucleation. Rod-like crystals appeared after 3–4 weeks and achieved maximum dimensions of ~0.5 × 0.2 × 0.1 mm. They belonged to the space group P1 with unit cell dimensions of a = 61.0 Å, b = 68.7 Å, c = 98.9 Å, α = 107.7°, β = 98.4°, and γ = 102.7° and contained four monomers in the asymmetric unit. Most likely the initial attempts at soaking crystals of space group $P2_1$ in solutions containing galactose resulted in a change of space group, thereby leading to the observed deterioration in the quality of the x-ray diffraction properties.

An x-ray data set from a crystal of the enzyme-sugar complex was collected to 2.3 Å resolution at 4 °C, processed with SAINT (Bruker AXS, Inc.), and scaled as described previously. This protein-substrate complex structure was solved via molecular replacement with the software package AMORE (36) and employing, as the search model, the x-ray coordinates for the apoenzyme. Iterative cycles of least square refinement with TNT (39) and manual manipulation with TURBO (40) reduced the R-factor to 16.9% for all observed data from 30.0 to 2.30 Å resolution. Refinement statistics are presented in Table II.

Quality of the X-ray Models—The models for both the apo- and sugar-bound forms of human galactose mutarotase refined to low R-factors with excellent overall stereochemistry as indicated in Table II. Electron density was visible for all of the polypeptide chains (Met-1 to Ala-342) in the asymmetric unit, regardless of the space group. In several of the monomers, the Gly-His motifs left behind from the intein construct were visible. Only the polypeptide chain backbone from Lys-249 to Lys-252 was somewhat weaker in each monomer. A Ramachandran plot reveals only one significant outlier in either the apoenzyme or the protein/galactose monomers, namely Asn-81 with average ϕ, ψ angles of 70° and −159°, respectively. The electron density corresponding to Asn-81 is unequivocal in each monomer, and, in fact, its side chain carboxamide group forms a hydrogen bond with the 2-hydroxyl group of bound β-D-galactose. This strained conformation is not a function of sugar binding because it is also observed in the apoenzyme model.

Shown in Fig. 1 is the electron density corresponding to one of the β-D-galactose moieties in the P1 asymmetric unit. Each of the four

[2] I. Rayment and G. Wesenberg, unpublished data.

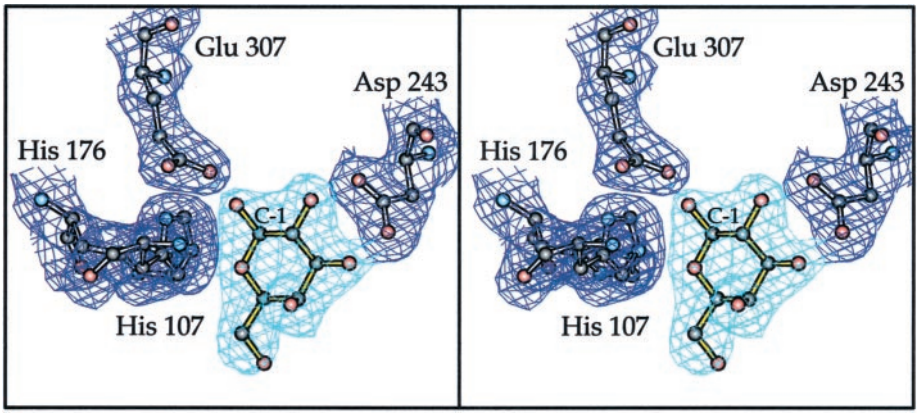

FIG. 1. **Representative electron density.** Electron density corresponding to the β-D-galactose moiety and surrounding amino acid residues is shown for monomer I in the x-ray coordinate file. The map was calculated with coefficients of the form $(2F_o - F_c)$, where F_o and F_c were the native and calculated structure factor amplitudes, respectively. The map was contoured at 1σ.

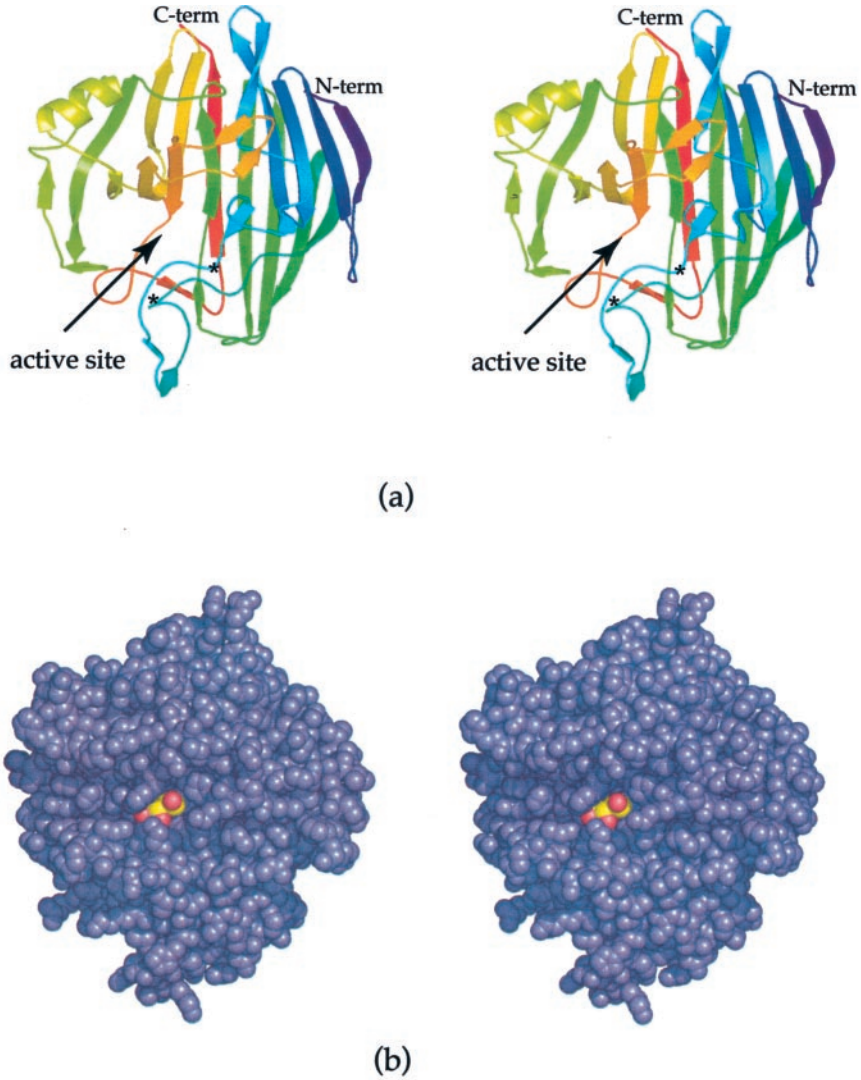

FIG. 2. **Structure of human galactose mutarotase.** A ribbon representation of the three-dimensional architecture exhibited by the apoenzyme is shown in *a*. For clarity, only the major strands of the β-sheet are displayed. *Asterisks* indicate the positions of *cis*-Arg-78 and *cis*-Pro-103. The location of the active site is depicted in *b* as a space-filling representation. Note that the 3-, 4-, and 6-hydroxyl groups of galactose, from *left* to *right* and indicated by the *red spheres*, are solvent-exposed. The view is approximately the same as displayed in *a*.

sugars in the asymmetric unit was modeled into the electron density map in the β-anomeric configuration. Excluding the C-6 hydroxyl oxygens, the average *B*-values for the sugars are between 31.0 and 39.4 Å^2. The C-6 hydroxyl oxygens refined to high *B*-values of 77.1, 89.3, 100, and 100 Å^2. These higher temperature factors most likely reflect the fact that there are no direct hydrogen-bonding interactions between the protein and this portion of the substrate.

RESULTS AND DISCUSSION

Crystals of the apo-form of galactose mutarotase belong to the space group $P2_1$ with two polypeptide chains per asymmetric unit. The α-carbons for these two monomers superimpose with an r.m.s.d. of 0.17 Å and, as such, are essentially identical within experimental error. Hence, for the sake of simplicity, the following discussion will only refer to monomer I in the x-ray coordinate file. The chitin-binding domain/intein construct employed for protein expression and purification left a residual glycine and a histidine residue at the N terminus. These two residues are well ordered in monomer I but are not visible in the electron density for monomer II.

Shown in Fig. 2*a* is a ribbon representation of the monomeric

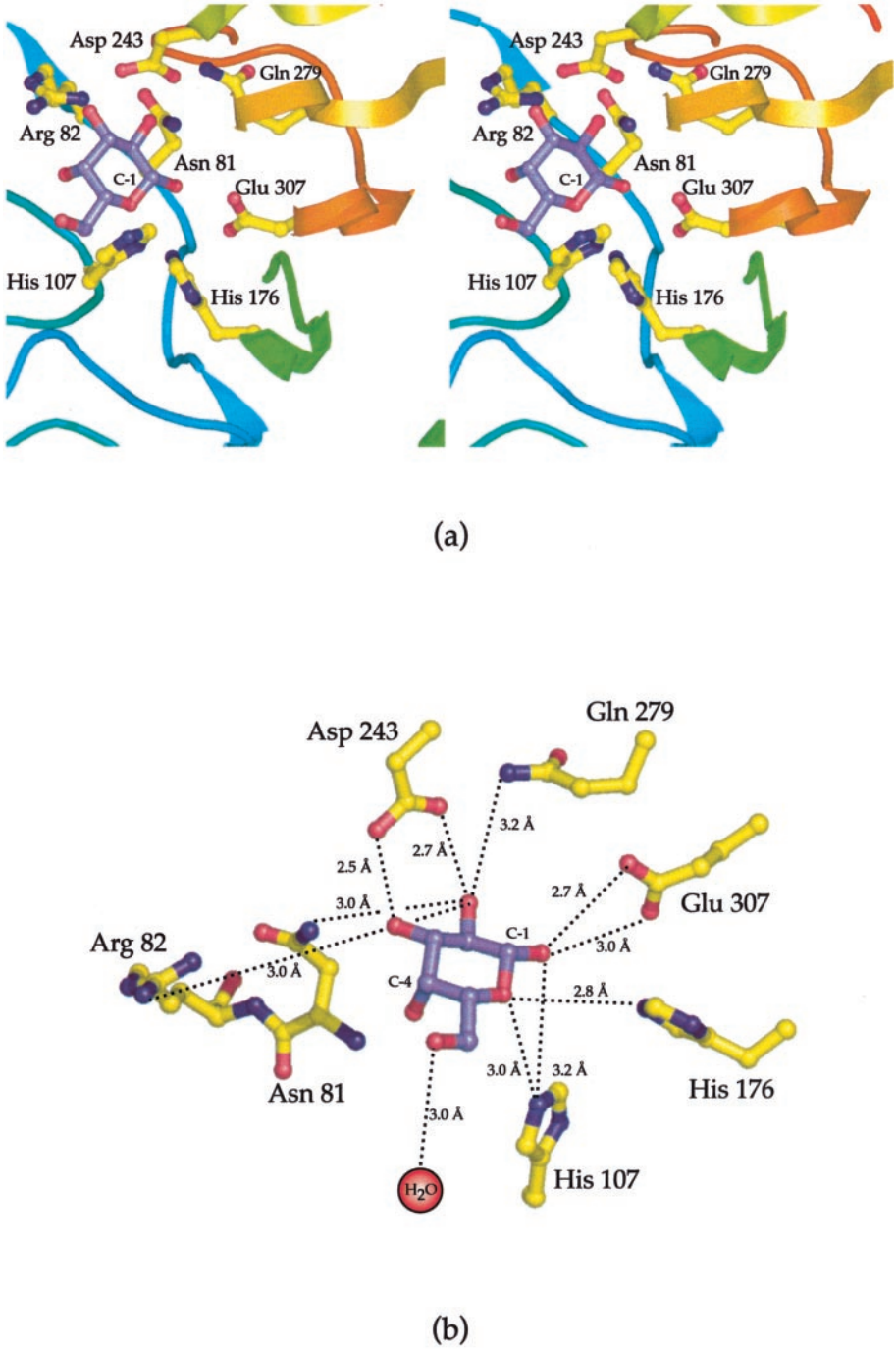

FIG. 3. **The active site for human galactose mutarotase.** A close-up stereo view of those amino acid residues involved in sugar binding is displayed in *a*. The color coding for the ribbon representation is the same as in Fig. 2. The sugar is *highlighted* in *grayish* bonds. Possible hydrogen bonding interactions between the protein and the ligand are shown schematically in *b*. The *dotted lines* indicate distances equal to or below 3.2 Å.

human enzyme, which has the overall dimensions of ~60 × 40 × 55 Å. The polypeptide chain folds into a complicated series of 29 β-strands ranging in length from 2 to 11 amino acid residues. These strands are connected by a number of classical reverse turns including 12 type I, 4 type I′, 6 type II, 1 type II′, 1 type III, and 1 type III′. There are two α-helical regions defined by Leu-62 to Leu-66 and Leu-230 to Leu-234. *cis*-Peptide bonds are observed at Arg-78 and Pro-103. Arg-78 is located in a coil region connecting β-strands 6 and 7, whereas Pro-103 is positioned in the loop between β-strands 9 and 10. The side chain of Arg-78 points away from the active site cleft.

When crystals of human galactose mutarotase are grown in the presence of D-galactose, the space group changes from $P2_1$ to P1 with four molecules in the asymmetric unit. These four monomers are, however, virtually identical, such that their α-carbons superimpose with r.m.s.d. values between 0.17 and 0.18 Å. The Gly-His motif at the N terminus is visible in the electron density for two of the four monomers in the asymmetric unit. Again, for the sake of simplicity, the following discussion will refer only to monomer I in the P1 asymmetric unit. Within experimental error, there are no significant structural changes in the enzyme that occur upon galactose binding. All main chain plus C-β atoms for the apo- and substrate-bound forms of galactose mutarotase correspond with a r.m.s.d. of 0.19 Å. The sugar moiety is situated in a shallow active site cleft with its 3-, 4-, and 6-hydroxyl groups somewhat solvent-exposed (as shown in Fig. 2*b*).

A close-up view of the region surrounding the sugar ligand is depicted in Fig. 3*a*. Those amino acid side chains responsible for anchoring the sugar to the protein include Asn-81, Arg-82, His-107, Asp-243, His-176, Gln-279, and Glu-307. A schematic diagram showing possible hydrogen bonding interactions be-

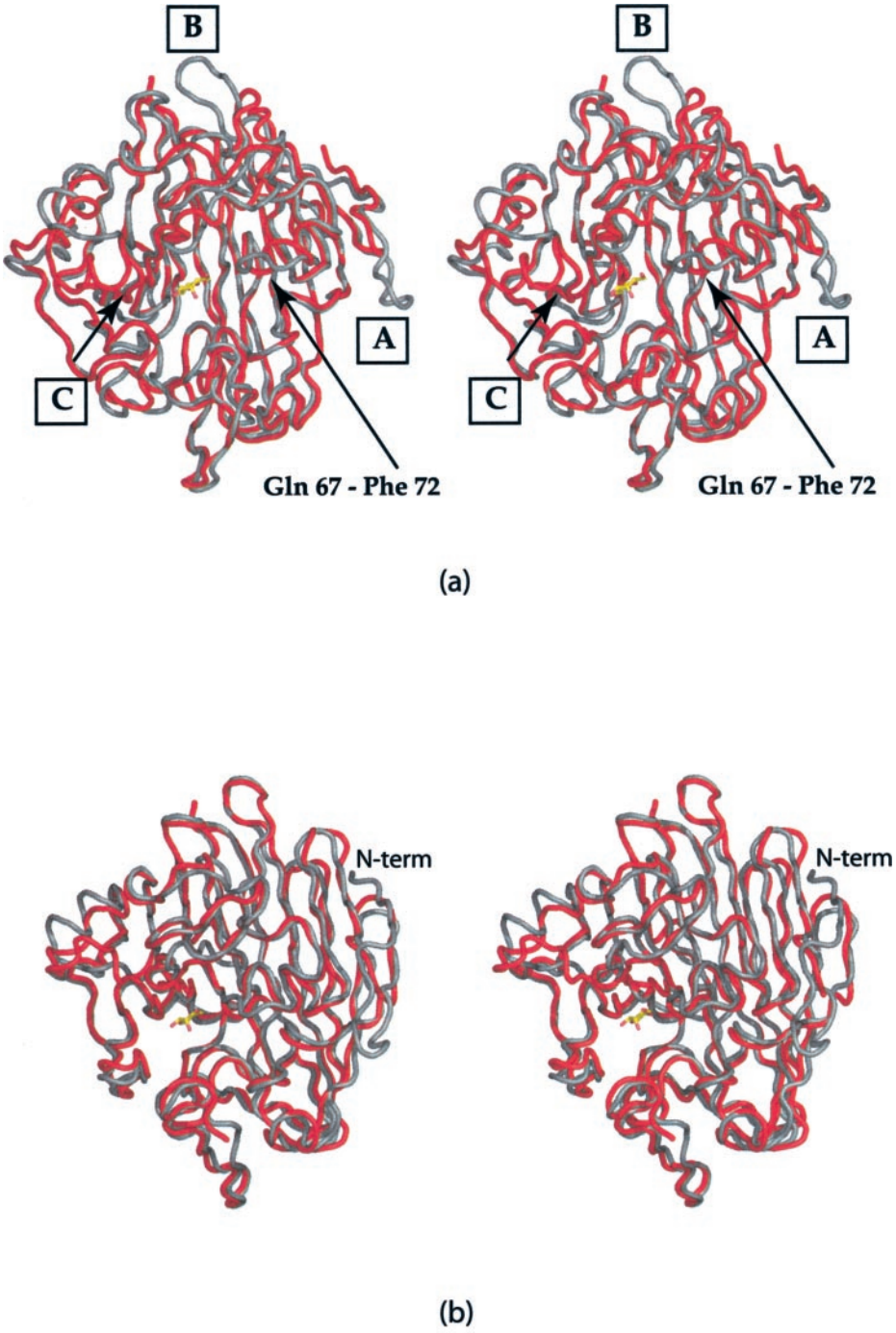

FIG. 4. **Comparison of the human, *L. lactis*, and *C. elegans* galactose mutarotases.** *a*, a superposition of the α-carbons for the human and *L. lactis* enzymes is shown in *black* and *red*, respectively. The *letters* indicate the positions of significant differences between the two proteins. The region defined by Gln-67 to Phe-72 in the human enzyme corresponds to Glu-56 to Pro-61 in the *L. lactis* mutarotase. X-ray coordinates for the *L. lactis* enzyme were from this laboratory. Shown in *b* is a superposition of the α-carbons for the human and *C. elegans* mutarotases, displayed in *black* and *red*, respectively. X-ray coordinates for the *C. elegans* protein were obtained from the Protein Data Bank (1LUR).

tween the protein and the ligand is presented in Fig. 3*b*. As predicted by Timson and Reece (30), Glu-307 is located within ~2.8 Å of the 1-hydroxyl group of galactose and thus is in the proper position to serve as the catalytic base for proton abstraction. Likewise, His-176 lies at ~2.8 Å from the ring oxygen and could possibly serve as a catalytic acid. The hydrogen bonding pattern displayed around the galactose moiety in the human enzyme is similar to that observed for the *L. lactis* mutarotase-sugar complex (24). The notable exceptions, however, are those interactions observed between the sugar and Asn-81 and Gln-279 in the human protein. The structurally equivalent residues in the *L. lactis* mutarotase are Gly-70 and Val-277, respectively. Recently, the structure of the apo-form of galactose mutarotase from *Caenorhabditis elegans* was solved to 1.85 Å resolution and the x-ray coordinates deposited in the Protein Data Bank (1LUR; Northeast Structural Genomics Target Wr66). Examination of the model for the *C. elegans* mutarotase demonstrates that the amino acid residues involved in sugar binding in the human protein, as *highlighted* in Fig. 3*b*, are conserved except for the replacement of Gln-279 with a histidine residue. It can thus be postulated that galactose will bind to the *C. elegans* protein in a similar fashion to that observed for the human and *L. lactis* enzymes.

The amino acid sequence similarity and identity between the human and *L. lactis* mutarotases is 49 and 32%, respectively. As expected from such high primary structural homology, these two enzymes have similar overall molecular architectures as shown in Fig. 4*a*. Indeed, the two mutarotases correspond with a r.m.s.d. of 1.2 Å for 307 structurally equivalent α-carbons. There are five regions where the two enzymes do differ significantly, however. As indicated by the letter *A* in Fig. 4*a*, there is a six-residue insertion beginning at Glu-11 in the human

protein. Another five-residue insertion, starting at Val-45, occurs in the human enzyme and is labeled *B* in Fig. 4*a*. Likewise, there are two insertions in the *L. lactis versus* the human enzyme: a four-residue insertion beginning at Asp-113 (not visible in the view given in Fig. 4*a*) and a five-residue insertion starting at Met-233 of the bacterial enzyme, which is labeled *C*. Strikingly, the region defined by Met-233 to Val-239 in the bacterial protein adopts an α-helical motif, which is missing in the human protein. Apart from these insertions/deletions, the polypeptide chains for the two enzymes differ elsewhere in the area delineated by Gln-67 to Phe-72, in the human mutarotase, and Glu-56 to Pro-61, in the *L. lactis* enzyme, as indicated in Fig. 4*a*. The differences observed in this region arise from the substitution of Pro-70 and Phe-72 with Ala-59 and Pro-61 in the human and bacterial proteins, respectively. Note that this region of polypeptide chain defines part of the active site cleft.

The mutarotase from *C. elegans* demonstrates an amino acid sequence identity of 33% with the human protein, and the two eukaryotic proteins superimpose with a r.m.s.d. of 1.0 Å for 301 equivalent α-carbons. Perhaps the most striking difference between the human and *C. elegans* enzymes occurs at the N terminus as can be seen in Fig. 4*b*. In the *C. elegans* protein, the first 17 residues are missing, thereby reducing the number of β-strands by one. Interestingly, the *cis*-peptide geometry observed at position 78 of the human enzyme is conserved in the *L. lactis* enzyme as *cis*-Pro-67 and as *cis*-Arg-63 in the *C. elegans* protein. Furthermore, although Pro-103 in the human enzyme is in the *cis* conformation, the peptide bonds for the prolines in the equivalent positions in the *C. elegans* and *L. lactis* mutarotases are in the *trans* conformation.

While the maintenance of the anomeric equilibrium of galactose is likely to be a major biochemical role for galactose mutarotase, it may also function in the metabolism of glucose and other sugars. Indeed, mutarotases have been shown to turn over various sugars including D-glucose, D-fucose, D-quinovose, L-arabinose, and D-xylose (8, 23, 33). With the gene sequence for the human enzyme now known, it will be possible to explore both its pattern of tissue expression and subcellular location. Undoubtedly, further biochemical investigations will shed additional light on the role of this fascinating enzyme in sugar metabolism.

REFERENCES

1. Holden, H. M., Rayment, I., and Thoden, J. B. (2003) *J. Biol. Chem.* **278,** 43885–43888
2. Petry, K. G., and Reichardt, J. K. (1998) *Trends Genet.* **14,** 98–102
3. Novelli, G., and Reichardt, J. K. (2000) *Mol. Genet. Metab.* **71,** 62–65
4. Kinoshita, J. H., Merola, L. O., and Dikmak, E. (1962) *Biochim. Biophys. Acta* **62,** 176–178
5. Dvornik, E., Simard-Duquesne, N., Krami, M., Sestanj, K., Gabbay, K. H., Kinoshita, J. H., Varma, S. D., and Merola, L. O. (1973) *Science* **182,** 1146–1148
6. Lin, L. R., Reddy, V. N., Giblin, F. J., Kador, P. F., and Kinoshita, J. H. (1991) *Exp. Eye Res.* **52,** 93–100
7. Tsakiris, S., Marinou, K., and Schulpis, K. H. (2002) *Pharmacol. Toxicol.* **91,** 254–257
8. Keston, A. S. (1963) *Arch. Biochem. Biophys.* **102,** 306–312
9. Wallenfels, K., Hucho, F., and Herrmann, K. (1965) *Biochem. Z.* **343,** 307–325
10. Wallenfels, K., and Herrmann, K. (1965) *Biochem. Z.* **343,** 294–306
11. Bouffard, G. G., Rudd, K. E., and Adhya, S. L. (1994) *J. Mol. Biol.* **244,** 269–278
12. Gatz, C., Altschmied, J., and Hillen, W. (1986) *J. Bacteriol.* **168,** 31–39
13. Poolman, B., Royer, T. J., Mainzer, S. E., and Schmidt, B. F. (1990) *J. Bacteriol.* **172,** 4037–4047
14. Mollet, B., and Pilloud, N. (1991) *J. Bacteriol.* **173,** 4464–4473
15. Maskell, D. J., Szabo, M. J., Deadman, M. E., and Moxon, E. R. (1992) *Mol. Microbiol.* **6,** 3051–3063
16. Erlandson, K. A., Delamarre, S. C., and Batt, C. A. (2001) *Appl. Environ. Microbiol.* **67,** 1445–1452
17. Bailey, J. M., Fishman, P. H., and Pentchev, P. G. (1966) *Science* **152,** 1270–1272
18. Bailey, J. M., Fishman, P. H., and Pentchev, P. G. (1967) *J. Biol. Chem.* **242,** 4263–4269
19. Bentley, R., and Bhate, D. S. (1960) *J. Biol. Chem.* **235,** 1219–1224
20. Keston, A. S. (1954) *Science* **120,** 355–356
21. Li, L. K. (1965) *Arch. Biochem. Biophys.* **110,** 156–162
22. Bailey, J. M., Pentchev, P. G., and Woo, J. (1965) *Biochim. Biophys. Acta* **94,** 124–129
23. Bailey, J. M., Fishman, P. H., and Pentchev, P. G. (1969) *J. Biol. Chem.* **244,** 781–788
24. Thoden, J. B., and Holden, H. M. (2002) *J. Biol. Chem.* **277,** 20854–20861
25. Jacobson, R. H., Zhang, X. J., DuBose, R. F., and Matthews, B. W. (1994) *Nature* **369,** 761–766
26. Bentley, R., and Bhate, D. S. (1960) *J. Biol. Chem.* **235,** 1225–1233
27. Hucho, F., and Wallenfels, K. (1971) *Eur. J. Biochem.* **23,** 489–496
28. Thoden, J. B., Kim, J., Raushel, F. M., and Holden, H. M. (2003) *Protein Sci.* **12,** 1051–1059
29. Beebe, J. A., Arabshahi, A., Clifton, J. G., Ringe, D., Petsko, G. A., and Frey, P. A. (2003) *Biochemistry* **42,** 4414–4420
30. Timson, D. J., and Reece, R. J. (2003) *FEBS Lett.* **543,** 21–24
31. Bailey, J. F., Fishman, P. H., Kusiak, J. W., Mulhern, S., and Pentchev, P. G. (1975) *Methods Enzymol.* **41,** 471–484
32. Beebe, J. A., and Frey, P. A. (1998) *Biochemistry* **37,** 14989–14997
33. Thoden, J. B., Kim, J., Raushel, F. M., and Holden, H. M. (2002) *J. Biol. Chem.* **277,** 45458–45465
34. Kabsch, W. (1988) *J. Appl. Crystallogr.* **21,** 916–924
35. Kabsch, W. (1988) *J. Appl. Crystallogr.* **21,** 67–71
36. Navaza, J. (1987) *Acta Crystallogr. Sect. A* **43,** 645–653
37. Jones, T. A. (1992) in *Molecular Replacement* (Dodson, E. J., Gover, S., and Wolf, W., eds) SERC Daresbury Laboratory, Warrington, UK
38. Kleywegt, G. J., and Jones, T. A. (1994) in *From First Map to Final Model* (Bailey, S., Hubbard, R., and Waller, D., eds) SERC Daresbury Laboratory, Warrington, UK
39. Tronrud, D. E., Ten Eyck, L. F., and Matthews, B. W. (1987) *Acta Crystallogr. Sect. A* **43,** 489–501
40. Roussel, A., and Cambillau, C. (1992) *Biographics* AFMB, Marseille, France